Proceedings of the
9th Graz Brain-Computer Interface Conference 2024

10.3217/978-3-99161-014-4-019

LOCALIZING NEURAL SOURCES IN THE CERVICAL SPINAL CORD

Markus E. Oberndorfer[1], Gernot R. Müller-Putz[1,2]

[1]Institute of Neural Engineering, Graz University of Technology, Graz, Austria
[2]BioTechMed Graz, Graz, Austria

E-mail: gernot.mueller@tugraz.at

ABSTRACT: Mapping neural activity along the spinal cord is a task that is hardly researched compared to human brain mapping. By identifying neural sources in the spinal cord and detecting unique activity patterns associated with various motor tasks or specific sensory input, it becomes possible to establish a baseline for healthy individuals. This could be utilized to classify spinal cord injuries or monitor changes in the spinal cord. This study demonstrates the effective application of an innovative approach to localizing the spinal sources of spinal cord potentials (SCPs) using the finite element method (FEM) to solve the forward problem and an abstraction of the sLORETA algorithm to identify the neural sources, which were induced by functional electrical stimulation (FES) on the forearms of healthy individuals.

INTRODUCTION

The field of human brain mapping, once limited to static classifications like Brodmann areas [1] based on structural composition, has now evolved into a dynamic process that allows researchers to gain more knowledge about the signal processing inside the brain. This dynamic process involves functional brain imaging, which is a set of imaging methods, e.g., functional magnetic resonance imaging (fMRI), magnetoencephalography (MEG) and electroencephalography (EEG) that can be applied to analyze real-time neural activity [2].

In the early work by Pfurtscheller et al. [3] brain patterns of hand movement imagination were used to allow a tetraplegic person to control an electrically driven hand orthosis. Additionally, this was one first work where multichannel EEG was projected onto the surface of a brain model in a BCI context. Since then, the field of functional brain imaging has evolved significantly. Different software packages, e.g., Brainstorm [4], EEGLab [5] and MNE [6] are currently available to visualize EEG data on a head model but also have large signal processing pipelines incorporated. Furthermore, those software packages allow to identify the neural sources in the brain by utilizing forward and inverse calculations. Forward computations involve modeling the propagation of electromagnetic fields from the neural sources within the brain to the scalp electrodes, taking into account the conductivity properties of the head tissues [7]. As for the inverse computations, there is a multitude of different algorithms available, which try to identify the location and magnitude of the neural sources for given EEG measurements [8]. These advancements have facilitated groundbreaking research in many fields, such as allowing researchers to identify conversely modulated gamma frequency bands in central sensorimotor areas during the human gait cycle [9] or proving that two different types of neural networks are active during rhythmic finger movements [10].

With this experience gained in human brain mapping, the way is paved to explore the mapping of sensory stimulations of the peripheral nervous system and motor tasks involving the limbs to the spinal cord. So far, there are hardly any publications that tackle the spinal cord mapping problem. In Stroman et al. [11], the neural activity changes in the lumbar spinal cord due to locally applied low temperatures on the skin were analyzed. The neural activity was recorded with fMRI. In Nierula et al. [12], a comprehensive recording of spinal cord somatosensory evoked potentials (SEPs) was performed in order to asses the functional architecture of somatosensory processing. A first attempt of sources localization of neural sources inside the spinal cord was done by Moffitt and Grill [13]. With their inverse model, they aimed to create an initial framework that can be used to obtain a more detailed map of the neuroanatomy of the spinal cord such that intraspinal, microstimulating electrodes are placed more effectively. However, they only simulated the signals using a basic cylinder structure, intended to mimic a simplified model of the spinal cord. Additionally, given that they were simulating invasive measurements of the spinal cord, they selected a relatively high artificial signal-to-noise ratio (SNR) compared to measurements typically obtained from the neck's skin. Currently, there is no work that uses non-invasively measured SCPs to find correlating neural sources. Therefore, the approach to spinal cord mapping herein is to identify neural sources in the spinal cord that are responsible for discernible potential changes following a predetermined stimulus.

Neural sources in the brain are believed to arise from synchronized synaptic activity [14]. Similar effects lead to measurable potential changes in the spinal cord, e.g., dorsal root potential (DRP), dorsal root reflex (DRR), primary afferent depolarization (PAD) [15]. These similarities provide additional support for choosing sLORETA as the preferred method for source localization in this initial

Published by
Verlag der Technischen Universität Graz

10.3217/978-3-99161-014-4-019

attempt.
Our objective was to demonstrate the presence of movement-related neural activity in the spinal cord through non-invasive recordings of spinal cord potentials. In particular, we aimed to identify neural responses elicited by afferent stimuli from functional electrical stimulation (FES) induced wrist movements.

MATERIALS AND METHODS

Data: We based our study on the data from Wimmer et al. [16]. Eight healthy participants underwent FES of the forearm, leading to a wrist extension. Simultaneously, a 16-channel EEG as well as 16-channel SCP recordings were performed (see Fig. 1). The FES-induced wrist movement was performed with a Microstim 8 stimulator (Krauth+Timmermann, Hamburg, Germany) and a stimulation frequency of $f_S = 35$Hz (pulse width of 300 μs). Only the raw 16-channel SCP recordings were considered for further analysis in this work. After processing the data with a high-pass ($f_H = 0.5$Hz), low-pass ($f_L = 60$Hz) and notch ($f_{N1} = 35$Hz, $f_{N2} = 50$Hz) filter, the signals were split into trials and averaged (for more detail see [16]).

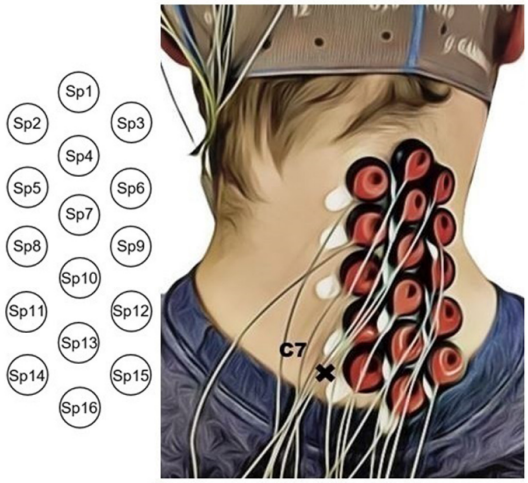

Figure 1: Electrode setup used in Wimmer et al. [16] to measure the Spinal Cord Potentials (SCPs). Image taken with permission from [16].

Geometrical model: To create the geometry for this model, the `NGSolve/NETGEN`-package in Python was used. For simplicity, only the following structures were added to the model: spinal cord, vertebraes, intervertebral discs, trachea, oesophagus and neck.

Forward problem: A Volume-Conduction model was used to describe the potential field distribution. To mathematically formulate this, Poisson's Equation was incorporated into the model:

$$\sigma \cdot (-\Delta V) = I_m \tag{1}$$

For some given current source density I_m and conductivity σ, the resulting potential V was calculated with the finite element method (FEM) [17]. The forward problem was implemented with the `NGSolve/NETGEN`-package in Python.
For simplicity, the conductivity of all materials was assumed to be homogeneous. Several publications [18–22] were taken into consideration to determine the conductivity values. The conductivity values are listed in Tab. 1.

Table 1: List of all materials with their respective conductivity.

Material	**Conductivity σ** [S/m]
Spine	0.22
Vertebrae	0.0014
Disc	0.008
Trachea	0.015
Oesophagus	0.015
Muscle (Neck)	0.01

Inverse problem: sLORETA [23] is widely acknowledged as a commonly utilized technique in EEG source localization, thereby validating its adoption in our proposed approach. Moreover, sLORETA was the preferred inverse algorithm method in [13]. In this study, we utilized a simplified version of the sLORETA algorithm. Derived from the original algorithm [23], the simplified version incorporates two key modifications: a cylinder-like geometry and the exclusion of deep sources.
The number of electrodes is defined as $N_E = 16$ and the number of dipoles assumed to occur in the cervical part of the spinal cord are defined as N_V.

Starting with the following equality

$$\mathbf{\Phi} = \mathbf{K}\mathbf{J} + c\mathbf{1} \quad , \tag{2}$$

in which $\mathbf{\Phi} \in \mathbb{R}^{N_E \times 1}$ represents the SCP measurements, $\mathbf{K} \in \mathbb{R}^{N_E \times (3N_V)}$ and $\mathbf{J} \in \mathbb{R}^{(3N_V)\times 1}$ are the leadfield matrix and the solution vector, respectively. The term $3N_V$ is due to the dimensionality of the model. While the positions of the dipoles remain fixed, it's important to consider the x-, y-, and z-directions individually for each electric dipole, as they can assume any orientation in space. The c variable introduces noise to the model. As customary, the forward problem is employed to compute the leadfield matrix $\mathbf{K}$. To obtain $\mathbf{J}$, the functional F has to be minimized with respect to $\mathbf{J}$ and c

$$F = ||\mathbf{\Phi} - \mathbf{K}\mathbf{J} - c\mathbf{1}||^2 + \alpha||\mathbf{J}||^2 \quad , \tag{3}$$

in which α is a regularization parameter.
The solution to this optimization problem is

$$\hat{\mathbf{J}} = \mathbf{T}\mathbf{\Phi} \quad , \tag{4}$$

in which $\hat{\mathbf{J}}$ is the solution vector containing all the neural sources' location, direction and magnitude. $\mathbf{T}$ is a pseudo-inverse of the leadfield matrix $\mathbf{K}$, calculated as

$$\mathbf{T} = \mathbf{K}^{\mathrm{T}}\mathbf{H}[\mathbf{H}\mathbf{K}\mathbf{K}^{\mathrm{T}}\mathbf{H} + \alpha\mathbf{H}]^{+} \quad , \tag{5}$$

in which $\mathbf{H}$ is the centering matrix.

Published by
Verlag der Technischen Universität Graz

10.3217/978-3-99161-014-4-019

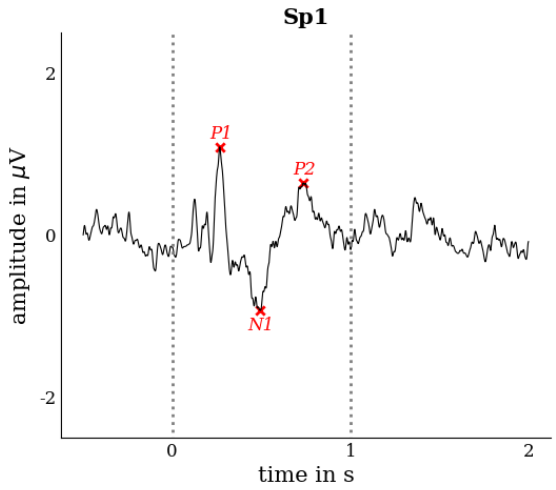

Figure 2: Average SCP obtained from one channel (Sp1) placed along the spine (Fig. 1). Three distinct peaks P1, N1, P2 are marked, as they are typical for potentials in the spinal cord.

More information regarding the calculations can be found in the original paper [23].

Optimization: From an optimization point of view, there are two hyperparameters that can be tuned. The first one is the regularization parameter $\alpha = [0.005, 0.01, 0.05, 0.1, 0.2, 0.35, 0.5]$ in Eq. 3. The second one is the number of dipoles $N_V = [21, 42, 63, 84, 105]$, which defines the size of the leadfield matrix $\mathbf{K}$. We computed the error functional F in Equation 3 for each combination of hyperparameters. Subsequently, we selected the hyperparameter combination that resulted in the lowest error for the final calculation.

RESULTS

After processing the data, the SCP signals exhibited a typical triphasic spike [24]. One of the 16 channels is shown representatively in Fig. 2. The characetristics of the triphasic spikes, calculated from all channels placed along the spine, are listed in Tab. 2.

Table 2: Amplitude and latency for the waveform points. Mean and standard deviation (SD) are calculated from the n=16 channels.

Waveform-point	Latency		Amplitude	
	Mean [ms]	SD [ms]	Mean [µV]	SD [µV]
P1 (n=16)	0.264	0.003	1.108	0.103
N1 (n=16)	0.487	0.004	-0.944	0.077
P2 (n=16)	0.739	0.005	0.708	0.097

The simplified neck geometry is visualized in Fig. 3. It captures only the most important features of a human neck that are necessary for the forward problem to deliver meaningful results. To show the functionality of the forward model, an axially oriented example dipole was inserted into the spinal cord (Fig. 4). A visualization of the solution vector $\hat{\mathbf{J}}$ is shown in Fig. 5 as red arrows. The vector length is normalized to the cylinder diameter

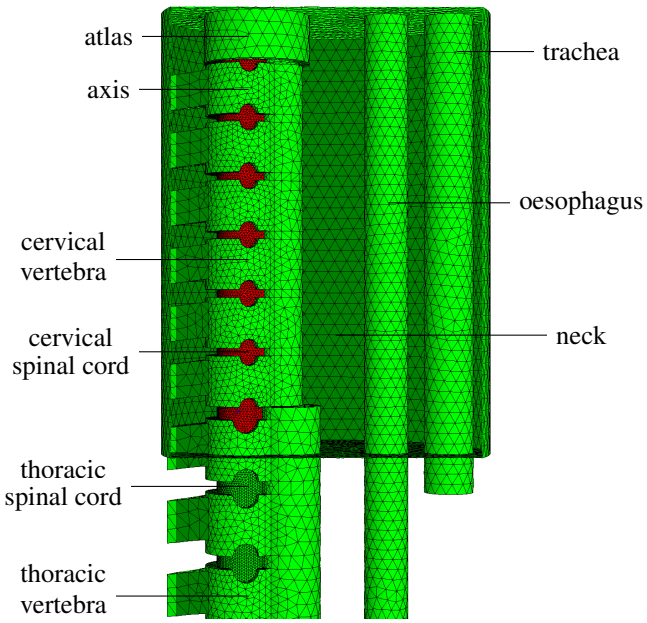

Figure 3: Neck part of the model dissected to reveal the spine, the trachea and the oesophagus with the cervical part of the spinal cord marked in red. The model incorporates a different structure for atlas and axis as well as different sizes for the vertebral bodies.

for each of the three solutions. The gray cylinder represents the neck.

The behaviour of the error functional F with respect to the hyperparameters α and N_V is shown in Fig. 6 for the first peak P1.

DISCUSSION

In this study, we successfully employed well-established methods for the forward and inverse computations to accurately localize neural sources within the spinal cord.

Based on the results of the forward problem, the potential field propagates primarily through the nervous tissue, indicating that the forward model works properly.

The nerves in the forearm are part of the Plexus Brachialis, which is a composition of spinal nerves C5-C8 and Th1 [25]. Since the large dipoles of P1 are located in the lower section of the cervical spinal cord, this result coincides with the anatomical structure of the nervous system. This is still partially true for the neural sources seen in points N1 and P2. Therefore, the results demonstrate the possibility of localizing the neural sources in the spinal cord. The influence of the hyperparameters (Fig. 6) on the error of the model indicates that $\alpha = 0.1$ offers the lowest error and that α has a more significant impact on the error than the number of dipoles N_V. Similar results were found for the N1 and P2 wave. Since the model does not capture much of the complexity the human body has to offer, these hyperparameter results should only be considered as initial guesses for future,

Published by
Verlag der Technischen Universität Graz

10.3217/978-3-99161-014-4-019

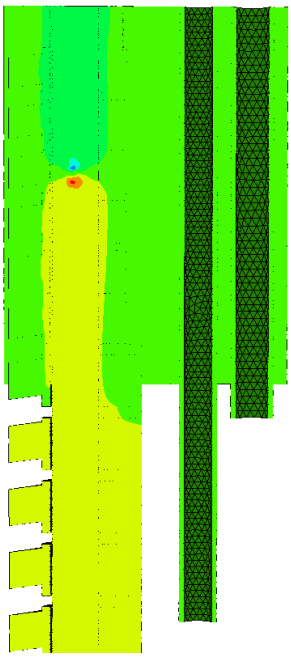

Figure 4: Visualization of the potential field distribution inside the model for an axially oriented electric dipole located in the spinal cord.

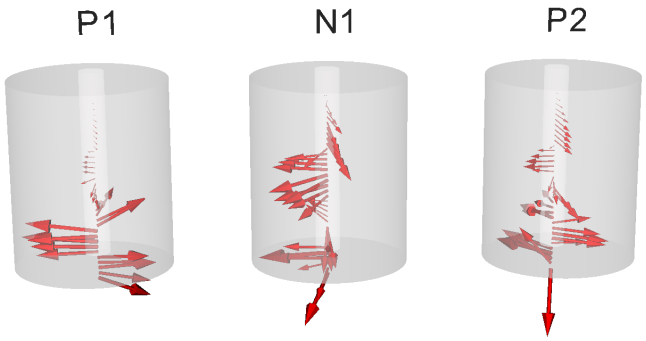

Figure 5: Solution of the source localization algorithm. The calculated dipoles are shown as red arrows originating from the spinal cord. The solution is shown for every wave P1, N1 and P2. The gray cylinder represents the neck.

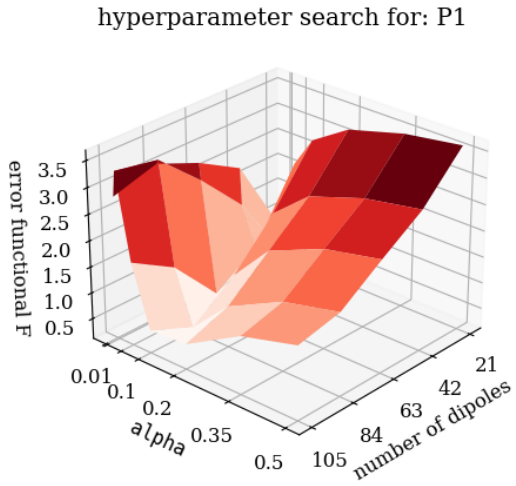

Figure 6: Behaviour of the error with respect to the two hyperparameters α and N_V.

more complex, models.
In this paper, only three points in time were compared. For actual mapping purposes, it would be appropriate to analyze the complete time domain to possibly obtain more differences in the neural activity induced by different stimuli.
Assuming that this mapping was conducted across numerous healthy individuals, it would establish a reference dataset that could be applied in various contexts and applications. For example, classifying the spinal cord injury level, monitoring disease progression through tracking changes in the spinal cord neural activity (e.g., in amyotrophic lateral sclerosis (ALS)) or changes during rehabilitation of spinal cord injured individuals.
Additionally, one could try to analyze the characteristics of the triphasic spike (latency and magnitude, Tab. 2) to distinguish between different motor tasks or stimuli. If more SCP recordings were available with a different stimulus, the characteristics might be slightly different and therefore, could be used for mapping.
This framework does come with a few limitations. First, the mathematical and geometrical model is very simple and does not capture the complexity oh the human physiology and anatomy, respectively. Especially, when it comes to large vessels like the Arteria carotis, which can distort the electric field. Further, the conductivity of biological tissue is anisotropic and is different for every human. Second, the measurements were taken from only one side of the neck and therefore, introduce a bias to the resulting sources. It is assumed that this bias is expressed in less precise directions of the dipoles. Third, since the stimulation of the forearm was performed with a 1s long 35Hz biphasic current pulse, the resulting SCPs are a summations of several consecutive stimuli, not just a single stimulus.
These considerations emphasize the importance of further refining both models and measurements in future research.

CONCLUSION

In this work, the feasibility of localizing electric dipoles in the cervical spinal cord based on recorded spinal cord potentials was demonstrated. By resolving the complicated challenges associated with the source localization problem, the findings reveal the potential for reasonably precise spatial identification within this neural region. These findings conclude that a spinal cord mapping of certain motor tasks or sensory stimuli is possible.

REFERENCES

[1] Strotzer M. One century of brain mapping using brodmann areas. Clinical Neuroradiology. 2009;19(3):179.
[2] Raichle ME. A brief history of human brain mapping. Trends in neurosciences. 2009;32(2):118–126.

Published by
Verlag der Technischen Universität Graz

10.3217/978-3-99161-014-4-019

[3] Pfurtscheller G, Guger C, Müller G, Krausz G, Neuper C. Brain oscillations control hand orthosis in a tetraplegic. Neuroscience letters. 2000;292(3):211–214.
[4] Tadel F, Baillet S, Mosher JC, Pantazis D, Leahy RM. Brainstorm: A user-friendly application for meg/eeg analysis. Computational intelligence and neuroscience. 2011;2011:1–13.
[5] Delorme A, Makeig S. Eeglab: An open source toolbox for analysis of single-trial eeg dynamics including independent component analysis. Journal of neuroscience methods. 2004;134(1):9–21.
[6] Gramfort A *et al.* Mne software for processing meg and eeg data. neuroimage. 2014;86:446–460.
[7] Hallez H *et al.* Review on solving the forward problem in eeg source analysis. Journal of neuroengineering and rehabilitation. 2007;4(1):1–29.
[8] Grech R *et al.* Review on solving the inverse problem in eeg source analysis. Journal of neuroengineering and rehabilitation. 2008;5(1):1–33.
[9] Seeber M, Scherer R, Wagner J, Solis-Escalante T, Müller-Putz GR. High and low gamma eeg oscillations in central sensorimotor areas are conversely modulated during the human gait cycle. Neuroimage. 2015;112:318–326.
[10] Seeber M, Scherer R, Müller-Putz GR. Eeg oscillations are modulated in different behavior-related networks during rhythmic finger movements. Journal of Neuroscience. 2016;36(46):11671–11681.
[11] Stroman PW, Tomanek B, Krause V, Frankenstein UN, Malisza KL. Mapping of neuronal function in the healthy and injured human spinal cord with spinal fmri. Neuroimage. 2002;17(4):1854–1860.
[12] Nierula B *et al.* Non-invasive multi-channel electrophysiology of the human spinal cord–assessing somatosensory processing from periphery to cortex. bioRxiv. 2022:2022–12.
[13] Moffitt MA, Grill WM. Electrical localization of neural activity in the dorsal horn of the spinal cord: A modeling study. Annals of biomedical engineering. 2004;32:1694–1709.
[14] Jackson AF, Bolger DJ. The neurophysiological bases of eeg and eeg measurement: A review for the rest of us. Psychophysiology. 2014;51(11):1061–1071.
[15] Giuliano LMP, Nunes KF, Manzano GM. The potentials recorded around the spinal cord: Different sides of the same dice. Revista Neurociências. 2013;21(3):449–454.
[16] Wimmer M, Kostoglou K, Müller-Putz GR. Measuring spinal cord potentials and cortico-spinal interactions after wrist movements induced by neuromuscular electrical stimulation. Frontiers in Human Neuroscience. 2022;16:858873.
[17] Zienkiewicz OC, Taylor RL, Zhu JZ. The finite element method: Its basis and fundamentals. Elsevier (2005).
[18] Vanrumste B. Eeg dipole source analysis in a realistic head model. Ph.D. dissertation. Ghent University. 2002.
[19] Jackson A, Travascio F, Gu W. Effect of mechanical loading on electrical conductivity in human intervertebral disk. Journal of biomechanical engineering. 2009;131:054505.
[20] Lee JH *et al.* In vivo electrical conductivity measurement of muscle, cartilage, and peripheral nerve around knee joint using mr-electrical properties tomography. Scientific Reports. 2022;12(1):73.
[21] Haueisen J *et al.* The influence of brain tissue anisotropy on human eeg and meg. Neuroimage. 2002;15(1):159–166.
[22] Huiskamp G, Vroeijenstijn M, Dijk R van, Wieneke G, Huffelen AC van. The need for correct realistic geometry in the inverse eeg problem. IEEE Transactions on Biomedical Engineering. 1999;46(11):1281–1287.
[23] Pascual-Marqui RD *et al.* Standardized low-resolution brain electromagnetic tomography (sloreta): Technical details. Methods Find Exp Clin Pharmacol. 2002;24(Suppl D):5–12.
[24] Yates BJ, Thompson FJ, Mickle PJ. Origin and properties of spinal cord field potentials. Neurosurgery. 1982;11(3):439–450.
[25] Orebaugh SL, Williams BA, *et al.* Brachial plexus anatomy: Normal and variant. The Scientific World Journal. 2009;9:300–312.

Published by
Verlag der Technischen Universität Graz